Journal of Molecular Structure 1034 (2013) 1–18

Contents lists available at SciVerse ScienceDirect

Journal of Molecular Structure

journal homepage: www.elsevier.com/locate/molstruc

Charge transfer complex of some nervous and brain drugs – Part 1: Synthesis, spectroscopic, analytical and biological studies on the reaction between haloperidol antipsychotic drugs with π-acceptors

Abeer A. El-Habeeb [a], Foziah A. Al-Saif [a], Moamen S. Refat [b,c,*]

[a] Department of Chemistry, Faculty of Science, Princess Nora Bint Abdul Rahman University, Riyadh, Saudi Arabia
[b] Department of Chemistry, Faculty of Science, Port Said, Port Said University, Egypt
[c] Department of Chemistry, Faculty of Science, Taif University, 888 Taif, Saudi Arabia

HIGHLIGHTS

- Synthesis of charge transfer complex of some nervous and brain drugs.
- Spectroscopic studies on the reaction between haloperidol with π-acceptors.
- The stoichiometry of these complexes was found to be 1:1 M ratio.
- These complexes were also tested for their antimicrobial activity against six different microorganisms.

ARTICLE INFO

Article history:
Received 24 June 2012
Received in revised form 21 August 2012
Accepted 24 August 2012
Available online 6 September 2012

Keywords:
Haloperidol
TCNQ
PA
Spectroscopic data
Charge transfer complex
Thermal analysis

ABSTRACT

Donor–acceptor interactions between the electron donor haloperidol (HPL) and π-acceptors like 7,7,8,8-tetracyanoquinodimethane (TCNQ) and picric acid (PA) have been studied spectrophotometrically in CH_3OH solvent. The donor–acceptor (charge transfer complexes) were discussed in terms of formation constant (K_{CT}), molar extinction coefficient (ε_{CT}), standard free energy (ΔG^o), oscillator strength (f), transition dipole moment (μ), resonance energy (R_N) and ionization potential (I_D). The stoichiometry of these complexes was found to be 1:1 M ratio and having the formulas [(HPL)(TCNQ)] and [(HPL)(PA)], respectively. The charge transfer interaction was successfully applied to determine of HPL drug using mentioned common π-acceptors also, the results obtained herein are satisfactory for estimation of HPL compound in the pharmaceutical form. The formed solid charge-transfer complexes were also isolated and characterized using elemental analysis, conductivity, (infrared, Raman, and ^{1}HNMR) spectra and X-ray powder diffraction (XRD). The experimental data of elemental analyses are in agreement with calculated data. The infrared spectra of both HPL complexes are confirming the participation of —OH of 4-hydroxy-1-piperidyl moiety in the donor–acceptor chelation. The morphological surface of the resulted charge transfer complexes were investigated using scanning electron microscopy (SEM). The thermogravimetric analysis (TG/DTG) and differential scanning calorimetry (DSC) techniques were performed to give knowledge about the thermal stability behavior of the synthesized charge transfer complexes. Thermodynamic parameters were computed from the thermal decomposition data. These complexes were also tested for their antimicrobial activity against six different microorganisms, and the results were compared with the parent drug.

1. Introduction

Haloperidol (Scheme 1) is a typical antipsychotic. It is in the butyrophenone class of antipsychotic medications and has pharmacological effects similar to the phenothiazines [1]. Haloperidol is an older antipsychotic used in the treatment of schizophrenia [2] and in the treatment of acute psychotic states and delirium. A long-acting decanoate ester is used as an injection given every 4 weeks to people with schizophrenia or related illnesses who have a poor compliance with medication and suffer frequent relapses of illness, or to overcome the drawbacks inherent to its orally administered counterpart that burst dosage increases risk or intensity of side effects. In some countries, injections of antipsychotics such as

* Corresponding author at: Department of Chemistry, Faculty of Science, Port Said, Port Said University, Egypt.
E-mail address: msrefat@yahoo.com (M.S. Refat).

0022-2860/$ - see front matter © 2012 Elsevier B.V. All rights reserved.
http://dx.doi.org/10.1016/j.molstruc.2012.08.045

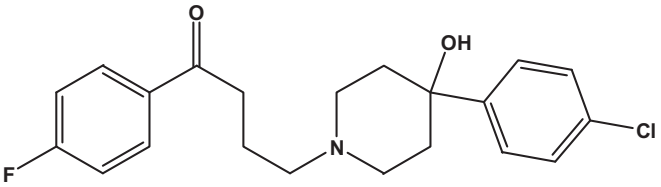

HPL

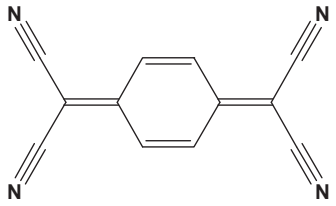

TCNQ

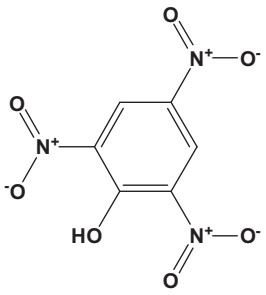

PA

Scheme 1. Haloperidol drug (HPL); IUPAC name 4-[4-(4-chlorophenyl)-4-hydroxy-1-piperidyl]-1-(4-fluorophenyl)-butan-1-one, acceptors; 7,7,8,8-tetracyanoquinodi methane (TCNQ) and picric acid (PA).

Table 1
Analytical and physical data for haloperidol (HPL) charge transfer complexes.

Compound Empirical formula (M. Wt.)	Color Before ppt	Color After ppt	Λm (Ω^{-1} cm^{-1} mol^{-1})	Elemental analysis (%) Found (Calcd.)			Yield (%)
				C	H	N	
HPL 375.86	White	White	10	67.11	6.17	3.73	–
[(HPL)(PA)]	Yellow	Yellow	45	53.39	4.21	9.12	89
(604.968)				(53.60)	(4.33)	(9.26)	
[(HPL)(TCNQ)]	Olive	Green	53	68.43	4.49	11.98	93
(579.043)	Green			(68.45)	(4.53)	(12.09)	

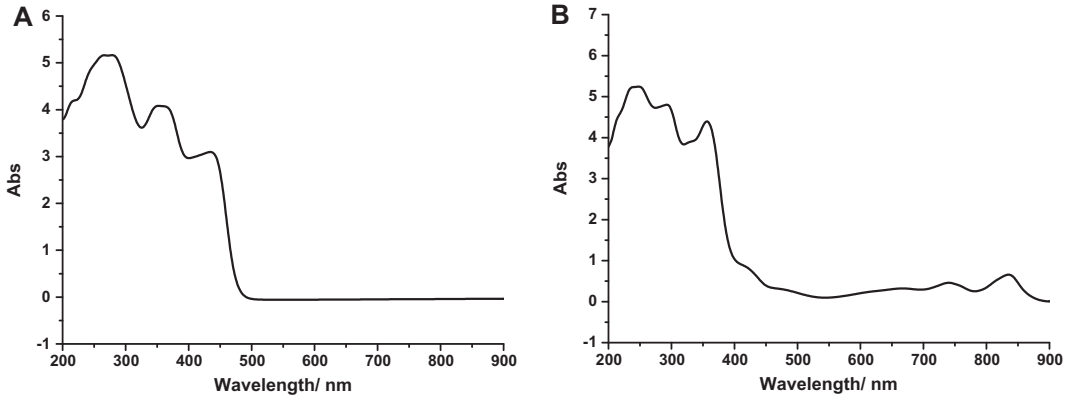

Fig. 1. Electronic absorption spectra of (A): [(HPL)(PA)] and [(HPL)(TCNQ)] charge transfer complexes in methanol solvent.

haloperidol can be ordered by a court at the request of a psychiatrist.

Donor acceptor complexation is an important phenomenon in biochemical and bioelectrochemical energy transfer process [3]. Charge transfer interactions between electron donors and acceptors are generally associated with the formation of intensely colored CT complexes which absorb radiation in the visible region [4]. Molecular complexation and structural recognition are important processes in biological systems; for example, drug action, enzyme catalysis, and ion transfers through lipophilic membranes all involve complexation [5]. Mulliken suggested that the formation of molecular complexes from two aromatic molecules can arise from the transfer of an electron from a π-molecular orbital of a Lewis base to vacant π-molecular orbital of a Lewis acid, with resonance between this dative structure and the no-band structure stabilizing the complex [6]. Mulliken also noted the possibility of complex for-

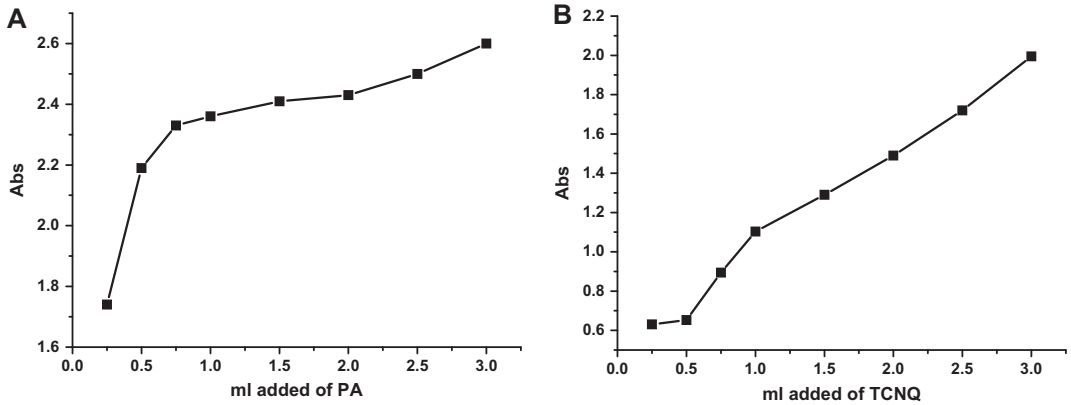

Fig. 2. Photometric titration spectra of (A): [(HPL)(PA)] and [(HPL)(TCNQ)] charge transfer systems in methanol solvent at refereed peaks of 447 nm and 357 nm, respectively.

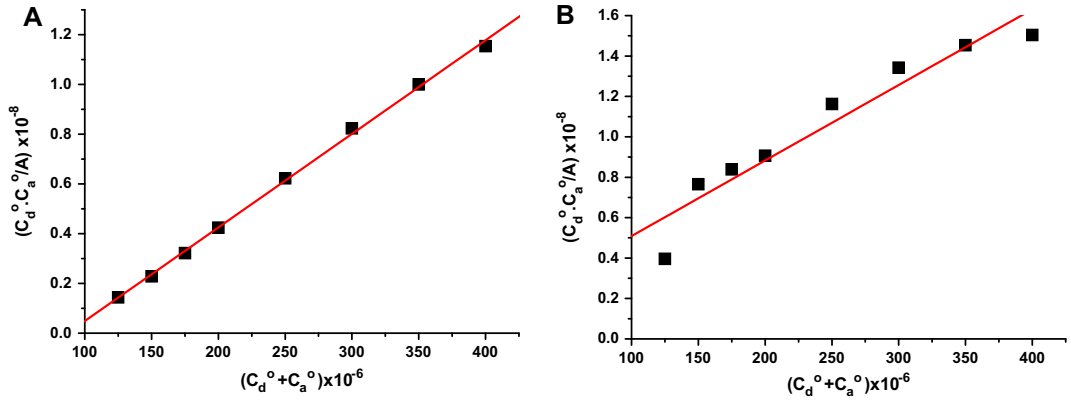

Fig. 3. The modified Benesi–Hildebrand plot of (A): [(HPL)(PA)] and [(HPL)(TCNQ)] charge transfer systems in methanol solvent at refereed peaks of 447 nm and 357 nm, respectively.

mation through the donation of an electron from a non-bonding molecular orbital in a Lewis base to a vacant π-orbital of an acceptor (n–π) [7] with resonance stabilization of the combination. The CT complexation is an important technique that is cheaper, simpler, and more efficient than the methods of drug determination described in the literature [8–16]. The solid charge transfer products of HPL with TCNQ and PA have not yet been reported in the literature; therefore the target of the present study was to investigate these reactions. Results of elemental analysis for all the HPL complexes are listed in Table 1. From this table, it can be seen that values found are in agreement with the calculated ones and the composition of the CT complexes are matched with the molar ratios presented from the photometric titration occurring between HPL and both π-acceptors. All of the complexes are insoluble in water and partially soluble in alcohols, but easily soluble in dimethyl formamide (DMF) and dimethylsulfoxide (DMSO).

2. Experimental

2.1. Chemicals and reagents

All chemicals and reagents used in this study were of analytical grade. Haloperidol was received from Egyptian International Pharmaceutical Industries Company EIPICO. Picric acid and 7,7,8,8-tetracyanoquinodimethane were obtained from Aldrich Chemical Company.

2.2. Synthesis of charge transfer complexes of HPL drug donor

The two haloperidol solid charge transfer complexes [(HPL)(PA)] and [(HPL)(TCN)] were synthesized as a yellow and green colors, respectively, by mixing a (3 mmol, 0.125 g) of haloperidol drug in 20 mL methanol to a 3 mmol of each acceptors; PA (0.0763 g) and (0.0680 g of TCNQ in 10 mL chloroform solvent. All mixtures were stirred for 45 min at room temperature and the

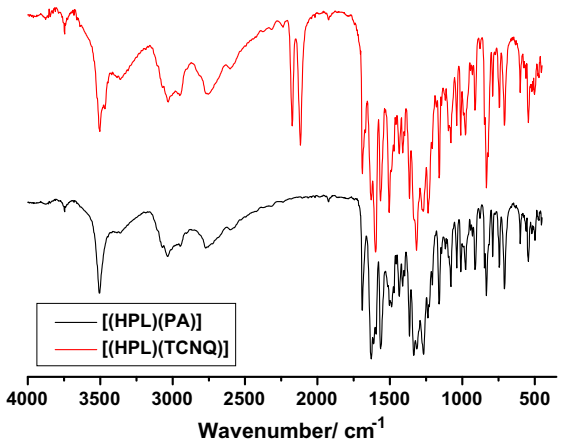

Fig. 4. IR spectra of [(HPL)(PA)] and [(HPL)(TCNQ)] charge transfer complexes.

Table 2
Spectorophotometric data of the HPL charge transfer systems in methanol.

λ_{max} (nm)	E_{CT} (eV)	K (l mol^{-1})	ε_{max} (l mol^{-1} cm^{-1})	f	μ	I_p	D	R_N	ΔG^o (25 °C) kJ mol^{-1}
[(HPL)(PA)]									
447	2.78	11468	26596	23	46.71	9.183	33	0.435	23163
[(HPL)(TCNQ)]									
357	3.48	27815	26738	23	41.85	10.05	33	0.546	25358

Table 3
Assignments of the IR spectral bands (cm^{-1}) of HPL, PA, TCNQ, [(HPL)(PA)], and [(HPL)(TCNQ)] charge transfer complexes.

HPL	PA	TCNQ	[(HPL)(acceptor)] CT-complexes		Assignments[b]
			PA	TCNQ	
3129	3416	3405	3502	3502	$\nu_{(O-H)}$
	3103		3357	3364	
2968	2980	3137	3030	3030	$\nu_{s(C-H)} + \nu_{as(C-H)}$ aliphatic
2955	2872	3050		2944	
2917		2969			$\nu_{s(C-H)} + \nu_{as(C-H)}$ aromatic
2839		2851			
2824					
–	–	–	2774	2761	Hydrogen bonding
			2597	2604	
–	–	2220	–	2171	$\nu_{(C\equiv N)}$
				2112	
1682	1861	–	1686	1692	$\nu_{(C=O);\ HPL}$
			1620		$\nu_{(C=O)}$; PA
1599	1632	1540	1567	1600	$\nu_{(C=C)}$
1505	1608		1489	1561	C—H deformation
1483	1529		1436	1495	
1471	1432		1403	1430	
1458				1404	
1411					
1378	1343	1352	1364	1364	$\nu_{(C-C)}$
1363	1312	1285	1332	1312	$\nu_{(C-N)}$
1314	1263	1205	1267	1267	$\nu_{(C-O)}$
1255	1150		1240	1233	CH, in-plane bend
1244			1150	1155	
1235					
1224					
1199					
1168					
1137	1086	1117	1076	1076	CH-deformation
1110	917	1044	1036	1042	$\nu_{(C-Cl)} + \nu_{(C-F)}$
1087	829	997	1004	1010	
1047	781	962	964	976	
1013	732	860	905	906	
1006	703	808	827	827	
998	652		787	787	
962			748	748	
951			702	702	
793			603	603	
742					
546	522	473	537	537	Skeletal vibration
500			499	491	CH bend
					CH out of plane bend
					CNC def.
					δNO_2

solid products were filtered off, washed with minimum amounts of chloroform and dried under vacuum over anhydrous $CaCl_2$.

2.3. Physical measurements and analytical estimations

The elemental analyses of carbon, hydrogen and nitrogen contents were performed using a Perkin Elmer CHN 2400. The molar conductivities of freshly prepared 1.0×10^{-3} mol/cm^3 dimethylsulfoxide (DMSO) solutions were measured for the dissolved HPL complexes using Jenway 4010 conductivity meter. The electronic absorption spectra of the resulted charge transfer complexes were recorded in methanol within 800–200 nm range using a Perkin–Elmer Precisely Lambda 25 UV/Vis double beam Spectrometer fitted with a quartz cell of 1.0 cm path length. Infrared spectra within the

range of 4000–400 cm^{-1} for the free reactants and the resulted CT-complexes were recorded from KBr discs using a Shimadzu FT-IR Spectrometer with 30 scans and 2 cm^{-1} resolution, while Raman laser spectra of samples were measured on the Bruker FT-Raman with laser 50 mW. ^{1}H NMR was recorded as DMSO solutions on a Bruker 600 MHz spectrometer using TMS as the internal standard. DSC-TG thermograms of the HPL charge transfer complexes were obtained on a NETZSCH STA 449F3. Samples in solid form were placed in aluminum pans with a pierced lid, and heated rate of 15 °C min^{-1} under a nitrogen flow. Scanning electron microscopy (SEM) images and Energy Dispersive X-ray Detection (EDX) were taken in Joel JSM-6390 equipment, with an accelerating voltage of 20 kV. The X-ray diffraction patterns for both haloperidol complexes were recorded on Bruker Advanced 8 X-ray powder diffraction, target Cu K_α radiation, step scan mode with step = 0.05° and counting time 3.0 s/step.

2.4. Antibacterial and antifungal activities

Antimicrobial activity of the tested samples was determined using a modified Kirby–Bauer disc diffusion method [17]. Briefly, 100 μL of the best bacteria/fungi were grown in 10 mL of fresh media until they reached a count of approximately108 cells/mL for bacteria or 105 cells/mL for fungi [18]. 100 μL of microbial suspension was spread onto agar plates corresponding to the broth in which they were maintained. Isolated colonies of each organism that might be playing a pathogenic role should be selected from primary agar plates and tested for susceptibility by disc diffusion method [19,20].

Of the many media available, National Committee for Clinical Laboratory Standards (NCCLS) recommends Mueller–Hinton agar due to: it results in good batch-to-batch reproducibility. Disc diffusion method for filamentous fungi tested by using approved standard method (M38-A) developed by the NCCLS [21] for evaluating the susceptibility of filamentous fungi to antifungal agents. Disc diffusion method for yeast developed standard method (M44-P) by the NCCLS [22]. Plates inoculated with filamentous fungi as *Aspergillus flavus* at 25 °C for 48 h; Gram (+) bacteria as *Staphylococcus aureus, Bacillus subtilis*; Gram (−) bacteria as *Escherichia coli*, *Pseudomonas aeruginosa* they were incubated at 35–37 °C for 24–48 h and yeast as *Candida albicans* incubated at 30 °C for 24–48 h and, then the diameters of the inhabitation zones were measured in millimeters [17]. Standard discs of Tetracycline (Antibacterial agent), Amphotericin B (Antifungal agent) served as positive controls for antimicrobial activity but filter disc impregnated with 10 μL of solvent (distilled water, chloroform, DMSO) were used as a negative control.

The agar used is Meuller–Hinton agar that is rigorously tested for composition and pH. Further the depth of the agar in the plate is a factor to be considered in the disc diffusion method. This method is well documented and standard zones of inhabitation have been determined for susceptible values. Blank paper disks (Schleicher & Schuell, Spain) with a diameter of 8.0 mm were impregnated 10 μL of tested concentration of the stock solutions. When a filter paper disc impregnated with a tested chemical is placed on agar the chemical will diffuse from the disc into the agar. This diffusion will place the chemical in the agar only around the disc. The solubility of the chemical and its molecular size will determine the size of the area of chemical infiltration around the disc. If an organism is placed on the agar it will not grow in the area around the disc if it is susceptible to the chemical. This area of no growth around the disc is known as a "Zone of inhibition" or "Clear zone". For the disc diffusion, the zone diameters were measured with slipping calipers of the National for Clinical Laboratory Standers [19]. Agar-based methods such as Etest disk diffusion can be good alternatives because they are simpler and faster than broth methods [23,24].

3. Results and discussions

3.1. Analytical data and conductivity measurements

The molecular weights, molecular formula, conductance, yield, color before and after precipitation as well as percentage of each carbon, hydrogen and nitrogen contents of haloperidol charge transfer complexes were listed in Table 1. The elemental analysis technique support the stoichiomerty between HPL (donor) and mentioned π-acceptors (PA and TCNQ) is 1:1. The chelation process occurs via —OH of 4-hydroxy-1-piperidyl moiety of haloperidol drug toward accepting centers. Conductivity meter type Jenway 4010 was used to measure conductivities of both charge transfer complexes of HPL donor in DMSO with 1.0×10^{-3} mol/dm^3 concentration. The conductivities of the free reactants were also measured at a similar condition in order to make comparison between the free donor and acceptors with those of its charge transfer complexes. The molar conductance of haloperidol CT-complexes was reported in Table 1. The molar conductance values of picric and TCNQ of HPL complexes have 45 and 53 Ω^{-1} cm^{-1} - mol^{-1}, respectively. The conductance values indicate that the charge transfer complexes have slightly electrolytic nature. Slightly electrolytic complexes assigned to the formation of posi-

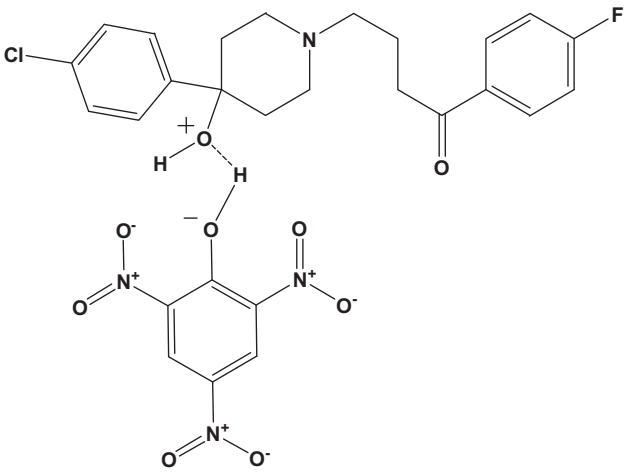

Scheme 2. Suggested structure of [(HPL)(PA)] complex.

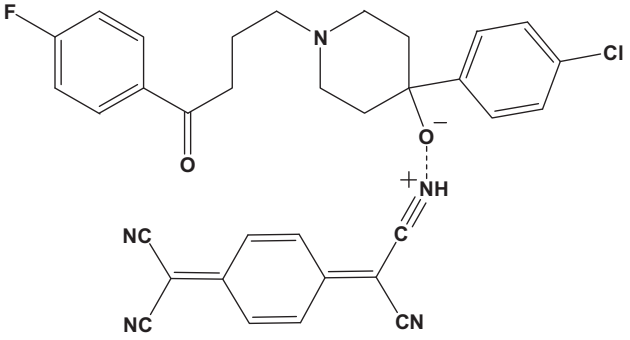

Scheme 3. Suggested structure of [(HPL)(TCNQ)] complex.

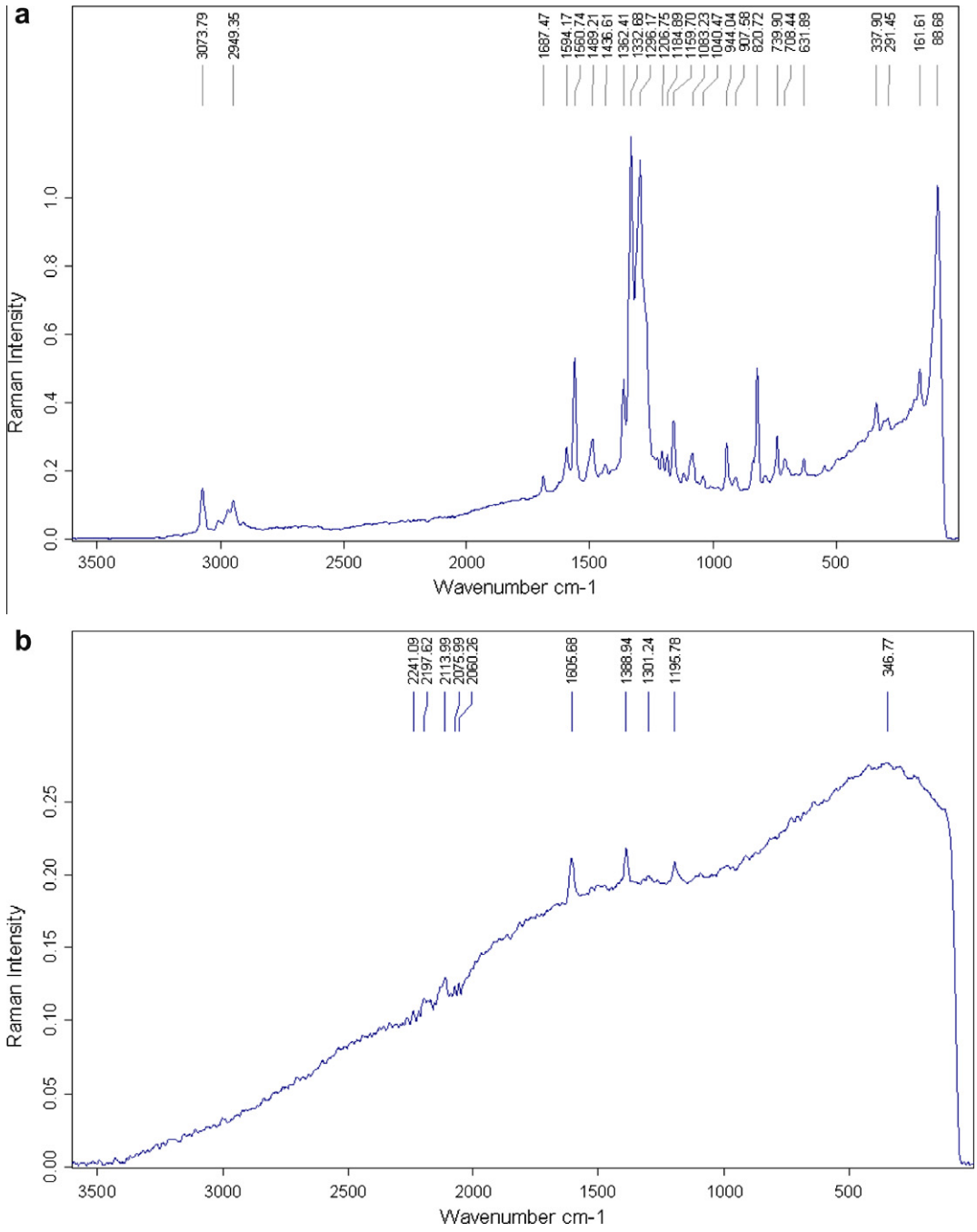

Fig. 5. Raman laser spectra of (a) [(HPL)(PA)] and (b) [(HPL)(TCNQ)] charge transfer complexes.

tive and negative datives anions under the donor–acceptor chelation [25].

3.2. Electronic spectra and physical data

The UV–vis spectra of PA and TCNQ of haloperidol charge-transfer complexes were measured in CH_3OH solvent. The CT complexes are formed by adding X mL of 5.0×10^{-4} M (PA or TCNQ) where (X = 0.25, 0.50, 0.75, 1.00, 1.50, 2.00, 2.50 and 3.00 mL) to 1.00 mL of 5.0×10^{-4} M HPL. The total volume of each system was completed to 5 mL with methanol solvent. The concentration of HPL in the reaction mixture was kept fixed at 1.00×10^{-4} M in CH_3OH solvent, while the concentration of PA or TCNQ was varied over the range of 0.25×10^{-4} M to 3.00×10^{-4} M for HPL/PA and HPL/TCNQ systems in CH_3OH solvent. These concentrations produce HPL:acceptor (PA or TCNQ) ratios extending along the range from 1:0.25 to 1:3.00. The electronic absorption spectra of the 1:1 ratios in methanol together with the reactants (PA and TCNQ) are shown in Fig. 1a and b. The spectra reveal the characterization of the real absorption bands which are not present in the spectra of free reactants. These bands are assigned at 447 nm and (357, 418, 738 and 837 nm) due to the CT complexes formed in the reaction of HPL with PA and TCNQ, respectively, in methanol solvent. Photometric titration curves based on these characterized absorption bands are given in Fig. 2a and b. These photometric titration curves were obtained according to known methods [26] by the plot of the absorbance against the X mL added of the PA or TCNQ as π-acceptors. The equivalence points shown in these curves clearly indicate

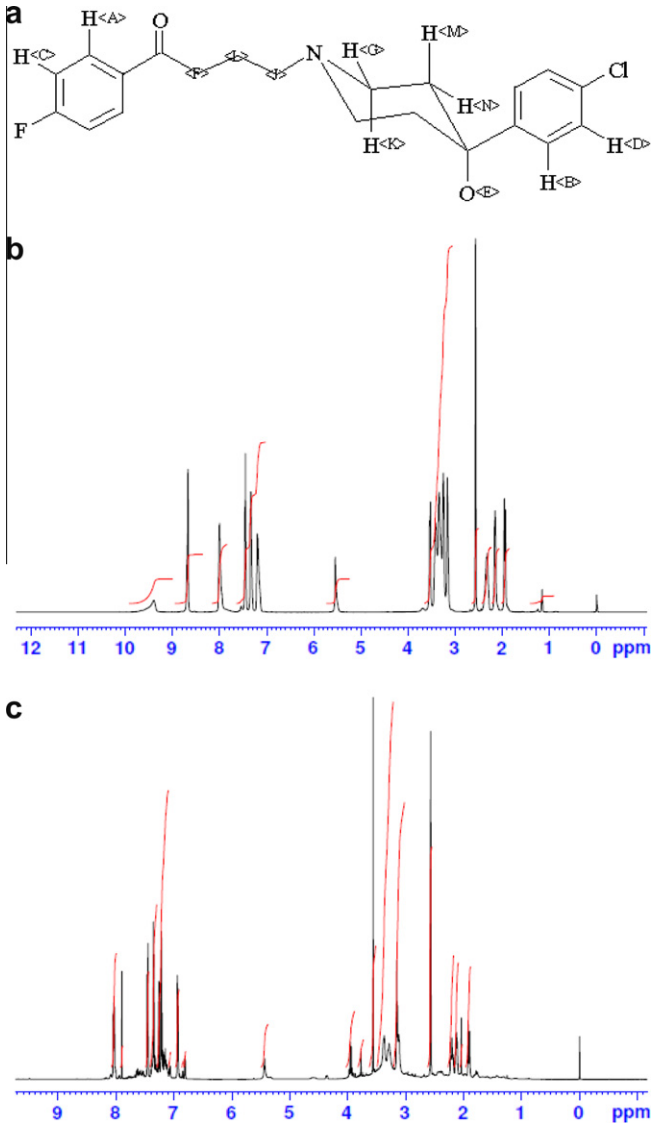

Fig. 6. Proton NMR spectra of (a) haloperidol free drug, (b) [(HPL)(PA)] complex, and (c) [(HPL)(TCNQ)] complex.

that the formed CT complexes between HPL and PA or TCNQ are 1:1. It was of interest to observe that the solvent has a pronounced effect on the spectral intensities of the formed [(HPL)(PA)] and [(HPL)(TCNQ)] complexes. The 1:1 modified Benesi–Hildebrand equation [27] was used in the calculations.

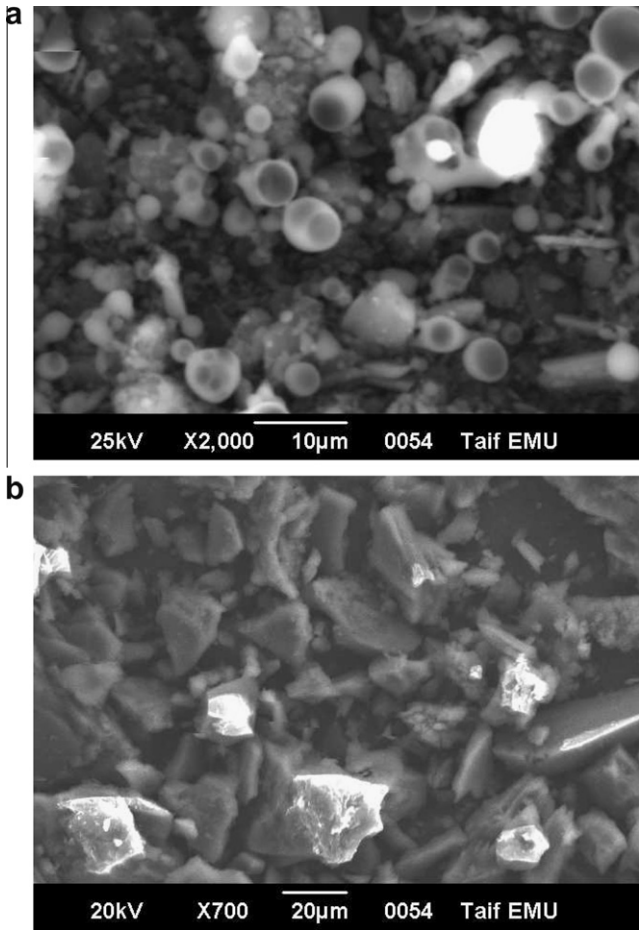

Fig. 7. SEM images spectra of (a) [(HPL)(PA)] and (b) [(HPL)(TCNQ)] complexes.

$$\frac{C_a^o C_d^o l}{A} = \frac{1}{K\varepsilon} + \frac{C_a^o + C_d^o}{\varepsilon} \quad (1)$$

where C_a^o and C_d^o are the initial concentrations of the acceptors (PA or TCNQ) and the donor HPL, respectively, K is a formation constant, ε is a molar extinction coefficient, and A is the absorbance of the definite bands around 447 and 357 nm for HPL/PA and HPL/TCNQ systems, respectively. The $C_a^o \cdot C_d^o/A$ values are plotted against the corresponding $C_a^o + C_d^o$ values, straight lines were obtained with a slope of $1/\varepsilon$ and intercept of $1/k\varepsilon$ as shown in Fig. 3a and b. The oscillator strength f was obtained from the approximate formula given in following equation [28]

$$f = (4.319 \times 10^{-9})\varepsilon_{max} \cdot \nu_{1/2} \quad (2)$$

Table 4
Assignments of the proton NMR spectral data (ppm) of HPL, [(HPL)(PA)], and [(HPL)(TCNQ)] charge transfer complexes.

Assignments		A	B	C	D	E	F	G	J	K	L	M	N
Shift (ppm)	HPL	8.08	7.37	7.36	7.34	4.85	2.98	2.58	2.36	2.34	1.85	1.67	1.47
	PA	8.00	7.40	7.30	7.10	5.50	3.20	2.60	2.40	2.20	1.90	–	1.20
		8.70					3.30						
		9.40					3.40						
							3.60						
		8.10	7.50	7.20	6.80	5.45	3.10	2.55	2.20	2.05	1.80	–	1.25
	TCNQ				6.90		3.30			2.15	1.90		
							3.35						
							3.55						
							3.80						
							3.90						

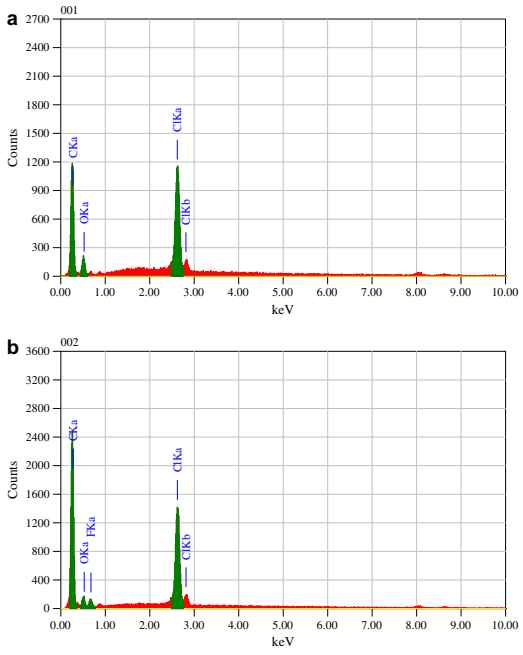

Fig. 8. EDX spectra of (a) [(HPL)(PA)] and (b) [(HPL)(TCNQ)] complexes.

where $v_{1/2}$ is the band-width for half-intensity in cm^{-1}. The oscillator strength values together with the corresponding dielectric constants, D, of the solvent used are given in Table 2. The trend of the values in this table reveals two facts:

The [(HPL)(PA)] and [(HPL)(TCNQ)] shows high values of both the equilibrium constant (K) and the extinction coefficient (ε). This high value of K reflects the high stability of the HPL complexes as a result of the expected high donation of the HPL consequently high value of ε which is known to have a high absorptivity values [29–31]. The transition dipole moment (μ) of the HPL complexes (Table 2) have been calculated from following equation [32]

$$\mu = 0.0958[\varepsilon_{max} v_{1/2}/v_{max}]^{1/2} \quad (3)$$

where $v_{1/2}$ is the bandwidth at half-maximum of absorbance, ε_{max} and v_{max} are the extinction coefficient and wavenumber at maximum absorption peak of the CT complexes, respectively. The ionization potential (I_p) of the free HPL donor was determined from the CT energies of the CT band of its complexes with different π-acceptors using the following relationships derived by Aloisi and Piganatro [33,34].

$$I_D\ (eV) = 5.76 + 1.53 \times 10^{-4} v_{CT} \quad (4)$$

where E_{CT} is the energy of the CT of the HPL complexes, the energy of the π–σ^*, n–σ^*, π–π^* or n–π^* interaction (E_{CT}) is calculated using following equation [32]

$$E_{CT}\ (eV) = (hv_{CT}) = 1243.667/\lambda_{CT}\ (nm) \quad (5)$$

where λ_{CT} is the wavelength of the complexation band. Determination of resonance energy (R_N), from Briegleb and Czekalla [35] theoretically derived the relation given in following equation

$$\varepsilon_{max}\ (l\ mol^{-1}\ cm^{-1}) = 7.7 \times 10^{-4}/[hv_{CT}/[R_N] - 3.5] \quad (6)$$

where ε_{max} is the molar extinction coefficient of the complex at the maximum CT absorption, v_{CT} is the frequency of the CT peak, and R_N is the resonance energy of the complex in the ground state, which obviously is a contributing factor to the stability constant of the complex (a ground state property). The values of R_N for the PA and TCNQ complexes under study are given in Table 2. The standard free energy changes of complexation (ΔG^o) were calculated from the association constants by following equation [36]

$$\Delta G^o = -2.303RT \log K_{CT} \quad (7)$$

where ΔG^o is the free energy change of the complexes (kJ mol^{-1}), R is the gas constant (8.314 J mol^{-1} K), T is the temperature in Kelvin degrees (273+ °C), and K_{CT} is the association constant of the complexes (l mol^{-1}) in different solvents at room temperature, the values thus calculated are represented in Table 2. The data of ΔG^o has a negative value according to the higher values of formation constant, and then the formation process of HPL charge transfer complexes is exothermic feature reactions.

3.3. Infrared and Raman spectra

The Infrared spectra of the reactants HPL, PA, TCNQ and the reaction products [(HPL)(PA)] and [(HPL)(TCNQ)] are presented in Fig. 4. Their band assignments are given in Table 3. The resulted charge transfer complexes produce from the interaction of HPL with PA and TCNQ are containing the characteristic bands of the HPL donor and acceptors (PA and TCNQ) with observed shift in the frequencies (Table 3), as well as some change in their bands intensities. This could be assigned to the expected symmetry and electronic structure changes upon the formation of the CT-complexes. The infrared interpretive for the formed CT-complexes are concluded as follows; The infrared spectra of the donor as well as the [(HPL)(PA)] formed CT complex is given in Fig. 4 and their band assignments are reported in Table 3. However, the appear-

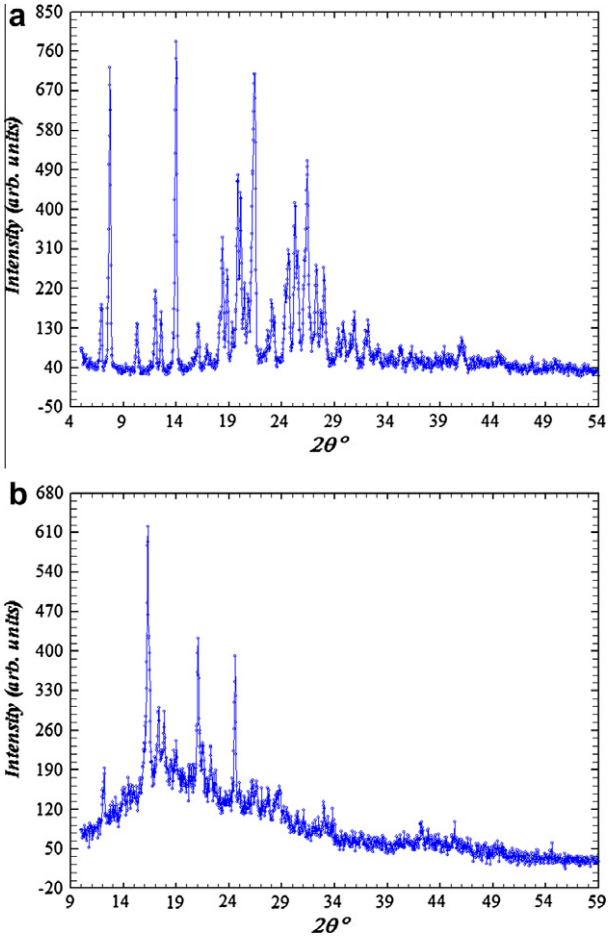

Fig. 9. XRD powder diffraction spectra of (a) [(HPL)(PA)] and (b) [(HPL)(TCNQ)] complexes.

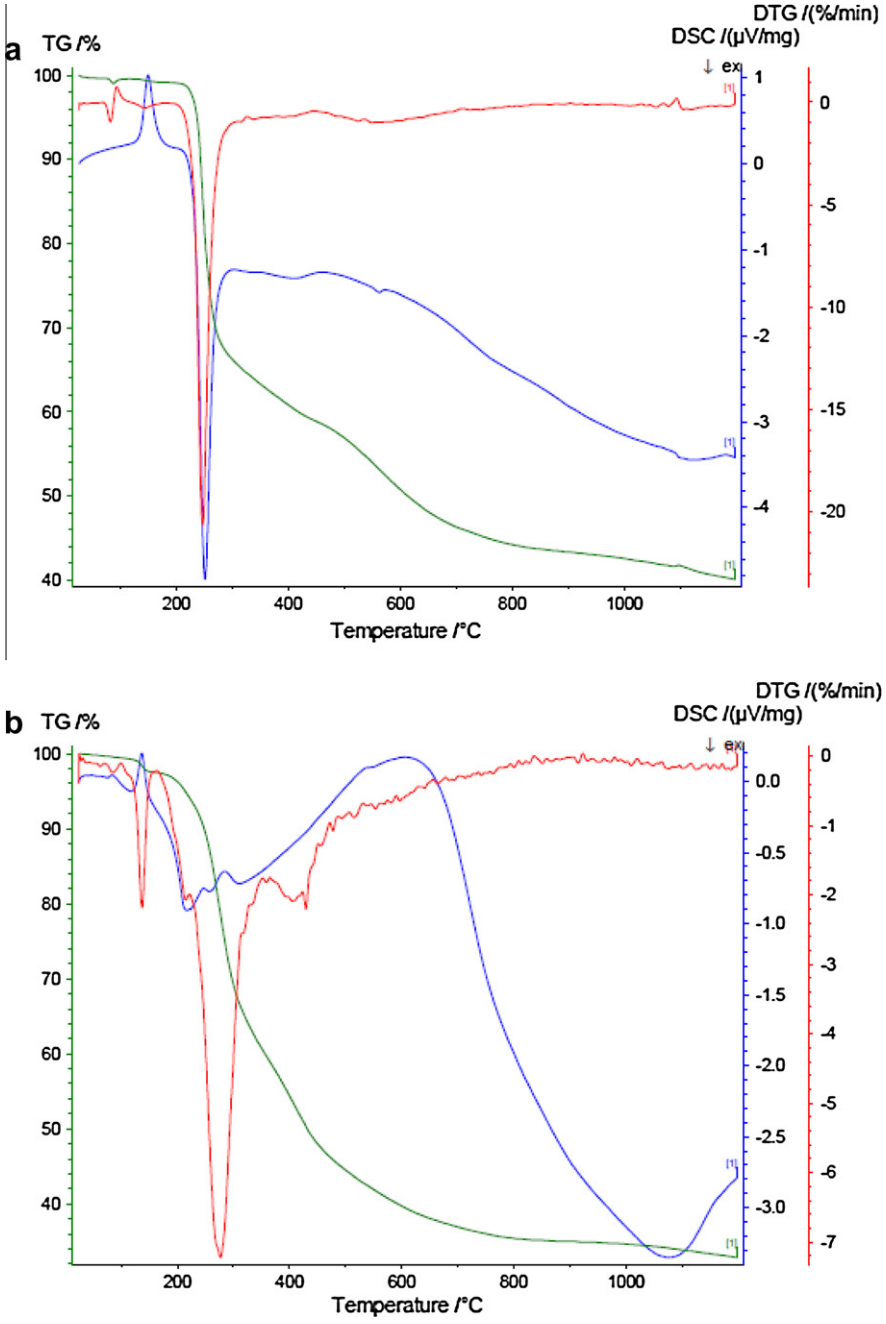

Fig. 10. TG/DTG and DSC curves of (a) [(HPL)(PA)] and (b) [(HPL)(TCNQ)] charge transfer complexes.

Table 5
Kinetic parameters of [(HPL)(PA)] and [(HPL)(TCNQ)] charge transfer complexes using the Coats–Redfern (CR) and Horowitz–Metzger (HM) equations.

Complex	DTG_{max}	Method	Parameter					r
			E ($J\ mol^{-1}$)	A (s^{-1})	ΔS ($J\ mol^{-1}\ K^{-1}$)	ΔH ($J\ mol^{-1}$)	ΔG ($J\ mol^{-1}$)	
PA	250	CR	1.29×10^5	3.91×10^{10}	-4.68×10^1	1.24×10^5	1.49×10^5	0.9041
		HM	1.34×10^5	3.15×10^{11}	-2.95×10^1	1.29×10^5	1.45×10^5	0.9021
TCNQ	280	CR	8.87×10^4	1.62×10^6	-1.31×10^2	8.41×10^4	1.57×10^5	0.9967
		HM	10.8×10^4	1.67×10^8	-9.27×10^1	1.03×10^5	1.55×10^5	0.9936

ance of a group of IR spectral bands in the spectrum of haloperidol picric acid CT complex supports the conclusion that a deformation of the electronic environment of haloperidol is occurred by accepting a proton from —OH of PA acceptor. The IR spectrum of PA complex is characterized by a group of bands appearing at 2774 and 2597 cm^{-1}, which are not appearing in the spectra of the free do-

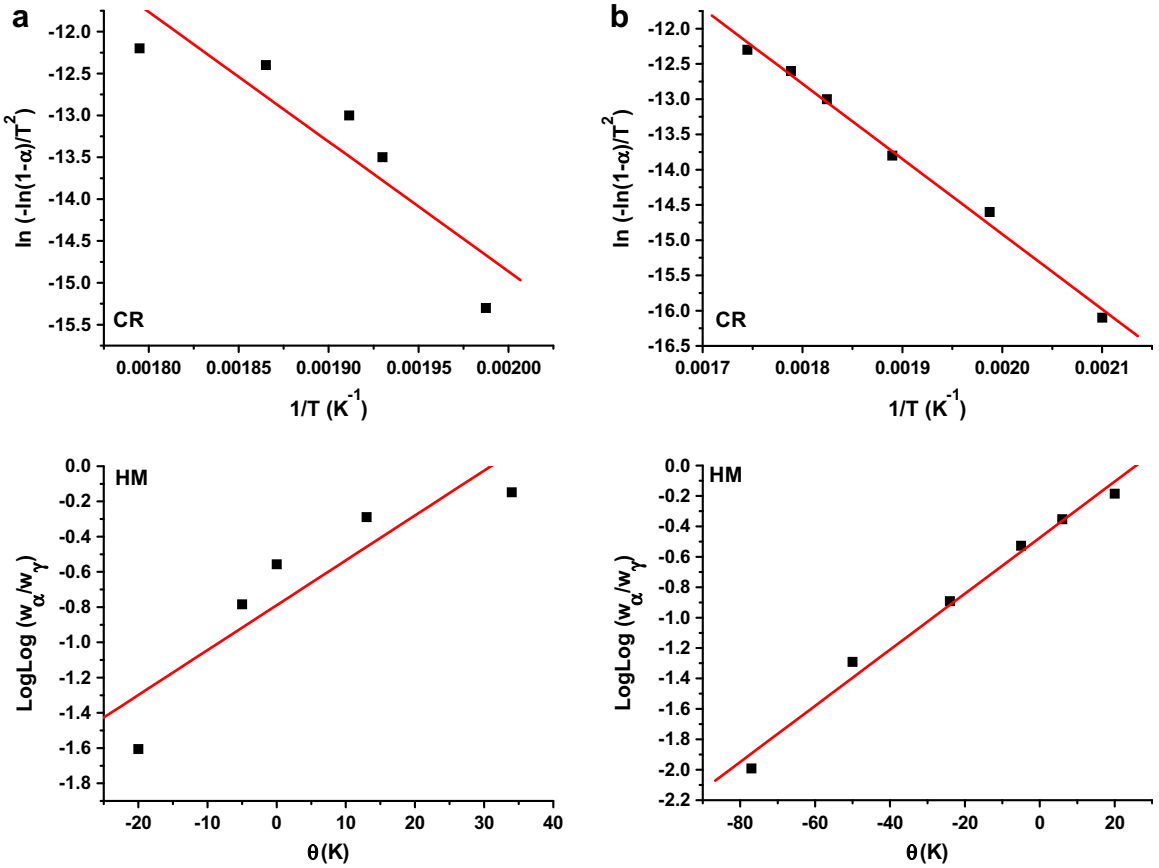

Fig. 11. Plots of Coats–Redfern (CR) and Horowitz–Metzger (HM) relations for (a) [(HPL)(PA)] and (b) [(HPL)(TCNQ)] charge transfer complexes.

nor and acceptors. These bands are attributed to the stretching vibration of a proton attached to the donation site of the donor [37]. These results caused by the intermolecular hydrogen bond occur in PA acceptor from —OH group to the basic center oxygen atom. The shift of the IR bands of the acceptor part to lower wavenumbers and those of the donor part to higher values reflects a donor to acceptor charge transfer of π–π^* interaction, $D_{HOMO} \rightarrow D_{LUMO}$ transition [38]. Accordingly, the hydrogen bonding between the donor and the acceptor, the suggested formula can be designed as Scheme 2.

Concerning of [(HPL)(TCNQ)] CT-complex, the IR spectrum of the solid reaction product contains the characteristic bands for both HPL (donor) and TCNQ (acceptor). The CN stretching of TCNQ show a drastic shift to lower value. The distinguish stretching vibration, ν(C≡N), of the free TCNQ is observed at 2220 cm^{-1} as single peak, but in the case of [(HPL)(TCNQ)] charge transfer complex, it means that after complexation, the two peaks at 2171 and 2112 cm^{-1} values are detected and having a strong band intensities. This shift is indicative of higher charge density on the cyano groups of TCNQ charge transfer complex. On the other hand, the —OH stretching band of HPL was shifted to higher frequencies in the spectrum of HPL/TCNQ complex. This is reasonable based on the increasing polarity of the —$^-$O—C≡NH^+ band during complexation. The interaction of TCNQ and haloperidol on the basis of infrared spectra can be suggested as Scheme 3. The conductance values at 1.0×10^{-3} molar concentrations indicated that these complexes have a small limit of conductivity. The data of conductivity confirms that these complexes have a positive and negative charge resulted from CT transition. The low conductivity values for the two CT-complexes may be due to intermolecular hydrogen bond formation.

Raman spectra of both [(HPL)(PA)] and [(HPL)(TCNQ)] complexes were performed and recorded differentiation that the picric acid complex has a seven regions with wavenumbers data 3074 cm^{-1}, 2949 cm^{-1}, 1687 cm^{-1}, (1594, 1560, 1489 and 1436 cm^{-1}), (1362, 1332, 1296, 1206, 1184, and 1159 cm^{-1}), (1083, 1040, 944, 907, 820, 739, and 708 cm^{-1}), and 631 cm^{-1} which assigned to ν(O—H), ν(C—H), ν(C=O), (ν(C=C) and C—H deformation), (ν(C—C), ν(C—N), ν(C—O), CH-in plane bend), (CH-deformation, ν(C—Cl), ν(C—F)) and (out-of-plane bend and $\delta(NO_2)$. The blue shifted caused to the stretching vibration band for —OH of HPL inside complexation led us to refer to the place of charge transfer chelation via —OH of HPL and —OH of picric acid. On the other hand, the spectrum of [(HPL)(TCNQ)] (Fig. 5b) has a sharp broadening with distorted in the stretching vibration band of cyano groups, this can be discussed under the knowledge that Raman analysis of fluorescent materials and compounds is a challenging task experimentally due to the overlap of fluorescence which, even when very weak, can overwhelm the inherently weak Raman scattering signal [39,40].

3.4. ^{1}H NMR spectra

The proton NMR spectra of the haloperidol free donor drug HPL and their charge transfer complexes of picric acid and TCNQ (Fig. 6) were recorded in DMSO-d_6 solvent using tetramethylsilane (TMS) as internal standard. The chemical shifts (δ) of the different types of protons of the ligand HPL and their charge transfer complexes are listed in Table 4. In details the chemical shifts of different kinds of protons in haloperidol drug can be justified in Fig. 6. The —OH signal of 4-hydroxy-1-piperidyl moiety for proton in position ⟨E⟩ (Fig. 6a) found at 4.85 ppm in the spectrum of the free haloperidol

Table 6
The values of bond lengths and bond angles of HPL, [(HPL)(PA)] and [(HPL)(TCNQ)] charge transfer complexes.

Adducts	Bond length			Bond angle		
	Atoms	Actual	Optimal	Atoms	Actual	Optimal
HPL	C(1)—C(2)	1.509	1.509	C(2)—C(1)—O(5)	122.331	122.5
	C(1)—O(5)	1.208	1.208	C(2)—C(1)—C(6)	114.835	115
	C(1)—C(6)	1.517	1.517	O(5)—C(1)—C(6)	122.832	123
	C(2)—C(3)	1.523	1.523	C(1)—C(2)—C(3)	109.998	110
	C(2)—H(44)	1.113	1.113	C(1)—C(2)—H(44)	108.8	108.8
	C(2)—H(45)	1.113	1.113	C(1)—C(2)—H(45)	108.8	108.8
	C(3)—C(4)	1.523	1.523	C(3)—C(2)—H(44)	109.409	109.41
	C(3)—H(42)	1.113	1.113	C(3)—C(2)—H(45)	109.409	109.41
	C(3)—H(43)	1.113	1.113	H(44)—C(2)—H(45)	109.4	
	C(4)—N(13)	1.438	1.438	C(2)—C(3)—C(4)	109.5	109.5
	C(4)—H(40)	1.113	1.113	C(2)—C(3)—H(42)	109.409	109.41
	C(4)—H(41)	1.113	1.113	C(2)—C(3)—H(43)	109.409	109.41
	C(6)—C(7)	1.42	1.42	C(4)—C(3)—H(42)	109.411	109.41
	C(6)—C(11)	1.42	1.42	C(4)—C(3)—H(43)	109.409	109.41
	C(7)—C(8)	1.42	1.42	H(42)—C(3)—H(43)	109.4	
	C(7)—H(49)	1.1	1.1	C(3)—C(4)—N(13)	109.5	109.5
	C(8)—C(9)	1.42	1.42	C(3)—C(4)—H(40)	109.409	109.41
	C(8)—H(46)	1.1	1.1	C(3)—C(4)—H(41)	109.409	109.41
	C(9)—C(10)	1.42	1.42	N(13)—C(4)—H(40)	108.8	
	C(9)—F(12)	1.32	1.32	N(13)—C(4)—H(41)	108.8	
	C(10)—C(11)	1.42	1.42	H(40)—C(4)—H(41)	109.4	
	C(10)—H(47)	1.1	1.1	C(1)—C(6)—C(7)	117.599	117.6
	C(11)—H(48)	1.1	1.1	C(1)—C(6)—C(11)	117.601	117.6
	N(13)—C(14)	1.438	1.438	C(7)—C(6)—C(11)	120	120
	N(13)—C(18)	1.438	1.438	C(6)—C(7)—C(8)	120	120
	C(14)—C(15)	1.523	1.523	C(6)—C(7)—H(49)	119.998	120
	C(14)—H(38)	1.113	1.113	C(8)—C(7)—H(49)	119.998	120
	C(14)—H(39)	1.113	1.113	C(7)—C(8)—C(9)	120	120
	C(15)—C(16)	1.514	1.514	C(7)—C(8)—H(46)	119.998	120
	C(15)—H(34)	1.113	1.113	C(9)—C(8)—H(46)	119.998	120
	C(15)—H(35)	1.113	1.113	C(8)—C(9)—C(10)	120.001	120
	C(16)—C(17)	1.514	1.514	C(8)—C(9)—F(12)	119.998	121
	C(16)—O(19)	1.421	1.421	C(10)—C(9)—F(12)	119.998	121
	C(16)—C(21)	1.497	1.497	C(9)—C(10)—C(11)	120	120
	C(17)—C(18)	1.524	1.523	C(9)—C(10)—H(47)	120	
	C(17)—H(32)	1.113	1.113	C(11)—C(10)—H(47)		
	C(17)—H(33)	1.113	1.113	C(6)—C(11)—C(10)	120	120
	C(18)—H(36)	1.113	1.113	C(6)—C(11)—H(48)	119.998	120
	C(18)—H(37)	1.113	1.113	C(10)—C(11)—H(48)	119.998	120
	O(19)—H(20)	0.942	0.942	C(4)—N(13)—C(14)	107.701	107.7
	C(21)—C(22)	1.42	1.42	C(4)—N(13)—C(18)	107.701	107.7
	C(21)—C(26)	1.42	1.42	C(14)—N(13)—C(18)	107.701	107.7
	C(22)—C(23)	1.42	1.42	N(13)—C(14)—C(15)	109.5	109.5
	C(22)—H(31)	1.1	1.1	N(13)—C(14)—H(38)	108.8	108.8
	C(23)—C(24)	1.42	1.42	N(13)—C(14)—H(39)	108.8	108.8
	C(23)—H(28)	1.1	1.1	C(15)—C(14)—H(38)	109.411	109.41
	C(24)—C(25)	1.42	1.42	C(15)—C(14)—H(39)	109.411	109.41
	C(24)—Cl(27)	1.719	1.719	H(38)—C(14)—H(39)	110.899	109.4
	C(25)—C(26)	1.42	1.42	C(14)—C(15)—C(16)	109.5	109.5
	C(25)—H(29)	1.1	1.1	C(14)—C(15)—H(34)	109.409	109.41
	C(26)—H(30)	1.1	1.1	C(14)—C(15)—H(35)	109.409	109.41
				C(16)—C(15)—H(34)	109.411	109.41
				C(16)—C(15)—H(35)	109.409	109.41
				H(34)—C(15)—H(35)	109.689	109.4
				C(15)—C(16)—C(17)	109.47	109.47
				C(15)—C(16)—O(19)	107.5	107.5
				C(15)—C(16)—C(21)	109.47	109.47
				C(17)—C(16)—O(19)	107.5	107.5
				C(17)—C(16)—C(21)	109.47	109.47
				O(19)—C(16)—C(21)	113.35	109.5
				C(16)—C(17)—C(18)	109.717	109.5
				C(16)—C(17)—H(32)	109.409	109.41
				C(16)—C(17)—H(33)	109.411	109.41
				C(18)—C(17)—H(32)	109.409	109.41
				C(18)—C(17)—H(33)	109.411	109.41
				H(32)—C(17)—H(33)	109.468	109.4
				N(13)—C(18)—C(17)	109.426	109.5
				N(13)—C(18)—H(36)	108.8	108.8
				N(13)—C(18)—H(37)	108.799	108.8
				C(17)—C(18)—H(36)	109.409	109.41
				C(17)—C(18)—H(37)	109.411	109.41
				H(36)—C(18)—H(37)	110.97	109.4
				C(16)—O(19)—H(20)	106.9	106.9

(*continued on next page*)

Table 6 (*continued*)

Adducts	Bond length			Bond angle		
	Atoms	Actual	Optimal	Atoms	Actual	Optimal
				C(16)—C(21)—C(22)	119.998	121.4
				C(16)—C(21)—C(26)	119.998	121.4
				C(22)—C(21)—C(26)	119.998	120
				C(21)—C(22)—C(23)	120	120
				C(21)—C(22)—H(31)	119.998	120
				C(23)—C(22)—H(31)	120	120
				C(22)—C(23)—C(24)	120	120
				C(22)—C(23)—H(28)	119.998	120
				C(24)—C(23)—H(28)	119.998	120
				C(23)—C(24)—C(25)	120	120
				C(23)—C(24)—Cl(27)	119.998	118.8
				C(25)—C(24)—Cl(27)	119.998	118.8
				C(24)—C(25)—C(26)	120	120
				C(24)—C(25)—H(29)	119.998	120
				C(26)—C(25)—H(29)	119.998	120
				C(21)—C(26)—C(25)	120	120
				C(21)—C(26)—H(30)	119.998	120
				C(25)—C(26)—H(30)	120	120
PA	C(1)—C(2)	1.509	1.509	C(2)—C(1)—O(5)	122.332	122.5
	C(1)—O(5)	1.208	1.208	C(2)—C(1)—C(6)	114.833	115
	C(1)—C(6)	1.517	1.517	O(5)—C(1)—C(6)	122.832	123
	C(2)—C(3)	1.523	1.523	C(1)—C(2)—C(3)	109.998	110
	C(2)—H(51)	1.113	1.113	C(1)—C(2)—H(51)	108.8	108.8
	C(2)—H(52)	1.113	1.113	C(1)—C(2)—H(52)	108.8	108.8
	C(3)—C(4)	1.523	1.523	C(3)—C(2)—H(51)	109.411	109.41
	C(3)—H(53)	1.113	1.113	C(3)—C(2)—H(52)	109.409	109.41
	C(3)—H(54)	1.113	1.113	H(51)—C(2)—H(52)	110.409	109.4
	C(4)—N(13)	1.438	1.438	C(2)—C(3)—C(4)	109.5	109.5
	C(4)—H(55)	1.113	1.113	C(2)—C(3)—H(53)	109.409	109.41
	C(4)—H(56)	1.113	1.113	C(2)—C(3)—H(54)	109.409	109.41
	C(6)—C(7)	1.42	1.42	C(4)—C(3)—H(53)	109.409	109.41
	C(6)—C(11)	1.42	1.42	C(4)—C(3)—H(54)	109.409	109.41
	C(7)—C(8)	1.42	1.42	H(53)—C(3)—H(54)	109.689	109.4
	C(7)—H(50)	1.1	1.1	C(3)—C(4)—N(13)	109.5	109.5
	C(8)—C(9)	1.42	1.42	C(3)—C(4)—H(55)	109.411	109.41
	C(8)—H(48)	1.1	1.1	C(3)—C(4)—H(56)	109.411	109.41
	C(9)—C(10)	1.42	1.42	N(13)—C(4)—H(55)	108.8	108.8
	C(9)—F(12)	1.32	1.32	N(13)—C(4)—H(56)	108.8	108.8
	C(10)—C(11)	1.42	1.42	H(55)—C(4)—H(56)	110.9	109.4
	C(10)—H(47)	1.1	1.1	C(1)—C(6)—C(7)	120	117.6
	C(11)—H(49)	1.1	1.1	C(1)—C(6)—C(11)	119.998	117.6
	N(13)—C(14)	1.438	1.438	C(7)—C(6)—C(11)	119.998	120
	N(13)—C(18)	1.438	1.438	C(6)—C(7)—C(8)	120	120
	C(14)—C(15)	1.523	1.523	C(6)—C(7)—H(50)	119.998	120
	C(14)—H(59)	1.113	1.113	C(8)—C(7)—H(50)	120	120
	C(14)—H(60)	1.113	1.113	C(7)—C(8)—C(9)	120.001	120
	C(15)—C(16)	1.523	1.523	C(7)—C(8)—H(48)	119.998	120
	C(15)—H(67)	1.113	1.113	C(9)—C(8)—H(48)	119.998	120
	C(15)—H(68)	1.113	1.113	C(8)—C(9)—C(10)	120.001	120
	C(16)—C(17)	1.523	1.523	C(8)—C(9)—F(12)	119.998	121
	C(16)—O(19)	1.402	1.402	C(10)—C(9)—F(12)	119.998	121
	C(16)—C(20)	1.497	1.497	C(9)—C(10)—C(11)	119.998	120
	C(17)—C(18)	1.525	1.523	C(9)—C(10)—H(47)	119.998	120
	C(17)—H(65)	1.113	1.113	C(11)—C(10)—H(47)	119.998	120
	C(17)—H(66)	1.113	1.113	C(6)—C(11)—C(10)	119.998	120
	C(18)—H(57)	1.113	1.113	C(6)—C(11)—H(49)	119.998	120
	C(18)—H(58)	1.113	1.113	C(10)—C(11)—H(49)	120	120
	O(19)—H(43)	0.992	0.992	C(4)—N(13)—C(14)	107.701	107.7
	O(19)—H(44)	0.992		C(4)—N(13)—C(18)	107.701	107.7
	C(20)—C(21)	1.42	1.42	C(14)—N(13)—C(18)	107.701	107.7
	C(20)—C(25)	1.42	1.42	N(13)—C(14)—C(15)	109.5	109.5
	C(21)—C(22)	1.42	1.42	N(13)—C(14)—H(59)	108.8	108.8
	C(21)—H(64)	1.1	1.1	N(13)—C(14)—H(60)	108.8	108.8
	C(22)—C(23)	1.42	1.42	C(15)—C(14)—H(59)	109.409	109.41
	C(22)—H(62)	1.1	1.1	C(15)—C(14)—H(60)	109.411	109.41
	C(23)—C(24)	1.42	1.42	H(59)—C(14)—H(60)	110.902	109.4
	C(23)—Cl(26)	1.719	1.719	C(14)—C(15)—C(16)	109.5	109.5
	C(24)—C(25)	1.42	1.42	C(14)—C(15)—H(67)	109.409	109.41
	C(24)—H(61)	1.1	1.1	C(14)—C(15)—H(68)	109.411	109.41
	C(25)—H(63)	1.1	1.1	C(16)—C(15)—H(67)	109.409	109.41
	O(27)—C(28)	1.41		C(16)—C(15)—H(68)	109.409	109.41
	O(27)—H(44)	0.992		H(67)—C(15)—H(68)	109.689	109.4
	C(28)—C(29)	1.42	1.42	C(15)—C(16)—C(17)	109.47	109.47

Table 6 (*continued*)

Adducts	Bond length			Bond angle		
	Atoms	Actual	Optimal	Atoms	Actual	Optimal
	C(28)—C(39)	1.42	1.42	C(15)—C(16)—O(19)	109.47	
	C(29)—N(30)	1.496	1.496	C(15)—C(16)—C(20)	109.47	109.47
	C(29)—C(33)	1.42	1.42	C(17)—C(16)—O(19)	109.47	
	N(30)—O(31)	1.316		C(17)—C(16)—C(20)	109.474	109.47
	N(30)—O(32)	1.143		O(19)—C(16)—C(20)	109.472	
	C(33)—C(34)	1.42	1.42	C(16)—C(17)—C(18)	109.666	109.5
	C(33)—H(46)	1.1	1.1	C(16)—C(17)—H(65)	109.409	109.41
	C(34)—N(35)	1.496	1.496	C(16)—C(17)—H(66)	109.409	109.41
	C(34)—C(38)	1.42	1.42	C(18)—C(17)—H(65)	109.409	109.41
	N(35)—O(36)	1.316		C(18)—C(17)—H(66)	109.409	109.41
	N(35)—O(37)	1.143		H(65)—C(17)—H(66)	109.521	109.4
	C(38)—C(39)	1.42	1.42	N(13)—C(18)—C(17)	109.426	109.5
	C(38)—H(45)	1.1	1.1	N(13)—C(18)—H(57)	108.799	108.8
	C(39)—N(40)	1.496	1.496	N(13)—C(18)—H(58)	108.8	108.8
	N(40)—O(41)	1.316		C(17)—C(18)—H(57)	109.411	109.41
	N(40)—O(42)	1.143		C(17)—C(18)—H(58)	109.409	109.41
				H(57)—C(18)—H(58)	110.972	109.4
				C(16)—O(19)—H(43)	106.999	107
				C(16)—O(19)—H(44)	109.47	
				H(43)—O(19)—H(44)	109.47	
				C(16)—C(20)—C(21)	120	121.4
				C(16)—C(20)—C(25)	119.998	121.4
				C(21)—C(20)—C(25)	119.998	120
				C(20)—C(21)—C(22)	120	120
				C(20)—C(21)—H(64)	119.998	120
				C(22)—C(21)—H(64)	119.998	120
				C(21)—C(22)—C(23)	120	120
				C(21)—C(22)—H(62)	119.998	120
				C(23)—C(22)—H(62)	119.998	120
				C(22)—C(23)—C(24)	120.001	120
				C(22)—C(23)—Cl(26)	119.998	118.8
				C(24)—C(23)—Cl(26)	119.998	118.8
				C(23)—C(24)—C(25)	119.998	120
				C(23)—C(24)—H(61)	120	120
				C(25)—C(24)—H(61)	119.998	120
				C(20)—C(25)—C(24)	120	120
				C(20)—C(25)—H(63)	119.998	120
				C(24)—C(25)—H(63)	119.998	120
				C(28)—O(27)—H(44)	109.47	
				O(27)—C(28)—C(29)	120	
				O(27)—C(28)—C(39)	119.998	
				C(29)—C(28)—C(39)	119.998	120
				C(28)—C(29)—N(30)	119.998	120
				C(28)—C(29)—C(33)	120	120
				N(30)—C(29)—C(33)	119.998	120
				C(29)—N(30)—O(31)	119.998	
				C(29)—N(30)—O(32)	120	
				O(31)—N(30)—O(32)	119.998	
				C(29)—C(33)—C(34)	120.001	120
				C(29)—C(33)—H(46)	119.998	120
				C(34)—C(33)—H(46)	119.998	120
				C(33)—C(34)—N(35)	119.998	120
				C(33)—C(34)—C(38)	120.001	120
				N(35)—C(34)—C(38)	119.998	120
				C(34)—N(35)—O(36)	119.998	
				C(34)—N(35)—O(37)	119.998	
				O(36)—N(35)—O(37)	119.998	
				C(34)—C(38)—C(39)	119.998	120
				C(34)—C(38)—H(45)	120	120
				C(39)—C(38)—H(45)	119.998	120
				C(28)—C(39)—C(38)	120	120
				C(28)—C(39)—N(40)	119.998	120
				C(38)—C(39)—N(40)	119.998	120
				C(39)—N(40)—O(41)	119.998	
				C(39)—N(40)—O(42)	119.998	
				O(41)—N(40)—O(42)	119.998	
				O(19)—H(44)—O(27)	109.472	
TCNQ	C(1)—C(2)	1.337	1.337	C(2)—C(1)—C(6)	120.001	120
	C(1)—C(6)	1.503	1.503	C(2)—C(1)—H(69)	119.998	120
	C(1)—H(69)	1.1	1.1	C(6)—C(1)—H(69)	119.998	120
	C(2)—C(3)	1.503	1.503	C(1)—C(2)—C(3)	120	120
	C(2)—H(60)	1.1	1.1	C(1)—C(2)—H(60)	120	120
	C(3)—C(4)	1.42	1.503	C(3)—C(2)—H(60)	119.998	120

(*continued on next page*)

Table 6 (*continued*)

Adducts	Bond length			Bond angle		
	Atoms	Actual	Optimal	Atoms	Actual	Optimal
	C(3)—C(7)	1.337	1.337	C(2)—C(3)—C(4)	120	120
	C(4)—C(5)	1.42	1.42	C(2)—C(3)—C(7)	119.998	120
	C(4)—H(59)	1.1	1.1	C(4)—C(3)—C(7)	119.998	120
	C(5)—C(6)	1.42	1.42	C(3)—C(4)—C(5)	120.001	120
	C(5)—H(68)	1.1	1.1	C(3)—C(4)—H(59)	119.998	120
	C(6)—C(8)	1.503	1.503	C(5)—C(4)—H(59)	119.998	120
	C(7)—C(12)	1.469	1.469	C(4)—C(5)—C(6)	120	120
	C(7)—C(14)	1.469	1.469	C(4)—C(5)—H(68)	120	120
	C(8)—C(9)	1.313	1.313	C(6)—C(5)—H(68)	119.998	120
	C(8)—C(10)	1.469	1.469	C(1)—C(6)—C(5)	119.998	120
	C(9)—N(16)	1.446		C(1)—C(6)—C(8)	120	120
	C(10)—N(11)	1.158	1.158	C(5)—C(6)—C(8)	119.998	120
	C(12)—N(13)	1.158	1.158	C(3)—C(7)—C(12)	119.998	120
	C(14)—N(15)	1.158	1.158	C(3)—C(7)—C(14)	119.998	120
	N(16)—O(36)	1.316		C(12)—C(7)—C(14)	119.998	120
	N(16)—H(17)	1.02	1.02	C(6)—C(8)—C(9)	119.998	120
	C(18)—C(19)	1.509	1.509	C(6)—C(8)—C(10)	119.998	120
	C(18)—O(22)	1.208	1.208	C(9)—C(8)—C(10)	119.998	120
	C(18)—C(23)	1.517	1.517	C(8)—C(9)—N(16)	179.684	
	C(19)—C(20)	1.523	1.523	C(8)—C(10)—N(11)	180	180
	C(19)—H(48)	1.113	1.113	C(7)—C(12)—N(13)	179.684	180
	C(19)—H(49)	1.113	1.113	C(7)—C(14)—N(15)	180	180
	C(20)—C(21)	1.523	1.523	C(9)—N(16)—O(36)	109.47	
	C(20)—H(50)	1.113	1.113	C(9)—N(16)—H(17)	109.47	
	C(20)—H(51)	1.113	1.113	H(17)—N(16)—O(36)	109.468	
	C(21)—N(30)	1.438	1.438	C(19)—C(18)—O(22)	122.332	122.5
	C(21)—H(52)	1.113	1.113	C(19)—C(18)—C(23)	114.833	115
	C(21)—H(53)	1.113	1.113	O(22)—C(18)—C(23)	122.832	123
	C(23)—C(24)	1.42	1.42	C(18)—C(19)—C(20)	110	110
	C(23)—C(28)	1.42	1.42	C(18)—C(19)—H(48)	108.8	108.8
	C(24)—C(25)	1.42	1.42	C(18)—C(19)—H(49)	108.8	108.8
	C(24)—H(47)	1.1	1.1	C(20)—C(19)—H(48)	109.409	109.41
	C(25)—C(26)	1.42	1.42	C(20)—C(19)—H(49)	109.407	109.41
	C(25)—H(44)	1.1	1.1	H(48)—C(19)—H(49)	110.409	109.4
	C(26)—C(27)	1.42	1.42	C(19)—C(20)—C(21)	109.5	109.5
	C(26)—F(29)	1.32	1.32	C(19)—C(20)—H(50)	109.409	109.41
	C(27)—C(28)	1.42	1.42	C(19)—C(20)—H(51)	109.409	109.41
	C(27)—H(45)	1.1	1.1	C(21)—C(20)—H(50)	109.409	109.41
	C(28)—H(46)	1.1	1.1	C(21)—C(20)—H(51)	109.411	109.41
	N(30)—C(31)	1.438	1.438	H(50)—C(20)—H(51)	109.689	109.4
	N(30)—C(35)	1.438	1.438	C(20)—C(21)—N(30)	109.5	109.5
	C(31)—C(32)	1.523	1.523	C(20)—C(21)—H(52)	109.411	109.41
	C(31)—H(56)	1.113	1.113	C(20)—C(21)—H(53)	109.412	109.41
	C(31)—H(57)	1.113	1.113	N(30)—C(21)—H(52)	108.799	108.8
	C(32)—C(33)	1.523	1.523	N(30)—C(21)—H(53)	108.799	108.8
	C(32)—H(66)	1.113	1.113	H(52)—C(21)—H(53)	110.899	109.4
	C(32)—H(67)	1.113	1.113	C(18)—C(23)—C(24)	119.998	117.6
	C(33)—C(34)	1.523	1.523	C(18)—C(23)—C(28)	119.998	117.6
	C(33)—O(36)	1.41		C(24)—C(23)—C(28)	120	120
	C(33)—C(37)	1.497	1.497	C(23)—C(24)—C(25)	120	120
	C(34)—C(35)	1.523	1.523	C(23)—C(24)—H(47)	119.998	120
	C(34)—H(64)	1.113	1.113	C(25)—C(24)—H(47)	120	120
	C(34)—H(65)	1.113	1.113	C(24)—C(25)—C(26)	120.001	120
	C(35)—H(54)	1.113	1.113	C(24)—C(25)—H(44)	119.998	120
	C(35)—H(55)	1.113	1.113	C(26)—C(25)—H(44)	120	120
	C(37)—C(38)	1.42	1.42	C(25)—C(26)—C(27)	120.001	120
	C(37)—C(42)	1.42	1.42	C(25)—C(26)—F(29)	119.998	121
	C(38)—C(39)	1.42	1.42	C(27)—C(26)—F(29)	119.998	121
	C(38)—H(63)	1.1	1.1	C(26)—C(27)—C(28)	119.998	120
	C(39)—C(40)	1.42	1.42	C(26)—C(27)—H(45)	120	120
	C(39)—H(58)	1.1	1.1	C(28)—C(27)—H(45)	119.998	120
	C(40)—C(41)	1.42	1.42	C(23)—C(28)—C(27)	120	120
	C(40)—Cl(43)	1.719	1.719	C(23)—C(28)—H(46)	119.998	120
	C(41)—C(42)	1.42	1.42	C(27)—C(28)—H(46)	119.998	120
	C(41)—H(61)	1.1	1.1	C(21)—N(30)—C(31)	107.702	107.7
	C(42)—H(62)	1.1	1.1	C(21)—N(30)—C(35)	107.701	107.7
				C(31)—N(30)—C(35)	107.699	107.7
				N(30)—C(31)—C(32)	109.502	109.5
				N(30)—C(31)—H(56)	108.799	108.8
				N(30)—C(31)—H(57)	108.8	108.8
				C(32)—C(31)—H(56)	109.409	109.41
				C(32)—C(31)—H(57)	109.409	109.41
				H(56)—C(31)—H(57)	110.9	109.4
				C(31)—C(32)—C(33)	109.5	109.5

Table 6 (*continued*)

Adducts	Bond length			Bond angle		
	Atoms	Actual	Optimal	Atoms	Actual	Optimal
				C(31)—C(32)—H(66)	109.409	109.41
				C(31)—C(32)—H(67)	109.412	109.41
				C(33)—C(32)—H(66)	109.409	109.41
				C(33)—C(32)—H(67)	109.409	109.41
				H(66)—C(32)—H(67)	109.687	109.4
				C(32)—C(33)—C(34)	109.47	109.47
				C(32)—C(33)—O(36)	109.47	
				C(32)—C(33)—C(37)	109.47	109.47
				C(34)—C(33)—O(36)	109.47	
				C(34)—C(33)—C(37)	109.474	109.47
				O(36)—C(33)—C(37)	109.47	
				C(33)—C(34)—C(35)	109.498	109.5
				C(33)—C(34)—H(64)	109.409	109.41
				C(33)—C(34)—H(65)	109.411	109.41
				C(35)—C(34)—H(64)	109.409	109.41
				C(35)—C(34)—H(65)	109.409	109.41
				H(64)—C(34)—H(65)	109.69	109.4
				N(30)—C(35)—C(34)	109.507	109.5
				N(30)—C(35)—H(54)	108.8	108.8
				N(30)—C(35)—H(55)	108.799	108.8
				C(34)—C(35)—H(54)	109.409	109.41
				C(34)—C(35)—H(55)	109.409	109.41
				H(54)—C(35)—H(55)	110.895	109.4
				N(16)—O(36)—C(33)	109.472	
				C(33)—C(37)—C(38)	120	121.4
				C(33)—C(37)—C(42)	119.998	121.4
				C(38)—C(37)—C(42)	119.998	120
				C(37)—C(38)—C(39)	120.001	120
				C(37)—C(38)—H(63)	119.998	120
				C(39)—C(38)—H(63)	120	120
				C(38)—C(39)—C(40)	120	120
				C(38)—C(39)—H(58)	119.998	120
				C(40)—C(39)—H(58)	119.998	120
				C(39)—C(40)—C(41)	120.001	120
				C(39)—C(40)—Cl(43)	119.998	118.8
				C(41)—C(40)—Cl(43)	119.998	118.8
				C(40)—C(41)—C(42)	120.001	120
				C(40)—C(41)—H(61)	119.998	120
				C(42)—C(41)—H(61)	119.998	120
				C(37)—C(42)—C(41)	120	120
				C(37)—C(42)—H(62)	119.998	120
				C(41)—C(42)—H(62)	120	120

donor is completely downfield in the spectra of both PA and TCNQ complexes, this support the sharing of the —OH group of (HPL) in charge transfer chelation with —OH for (PA) and —CN for (TCNQ) of acceptors via intermolecular hydrogen bond. In case of [(HPL)(PA)] complex the proton NMR spectrum showed signal at 9.40 ppm is actually shifted downfield due to the involvement of —OH proton (picric acid) towards the —OH proton of 4-hydroxy-1-piperidyl moiety.

3.5. Scanning electron microscopy, EDX, and XRD studies

Microstructure and morphology of the synthesized charge transfer complexes were analyzed by electronic microscopy SEM, EDX and XRD, the recorded images and diffractometry are shown in Fig. 7–9, respectively. The electron micrograph shows that morphology of the different haloperidol charge transfer complexes depend on the acceptor present, due to the different chemical structure of the adducts produced. The EDX spectra (Fig. 8a and b) corroborates the presence of carbon, oxygen, halogens (chlorine and fluorine) in the haloperidol adducts. The uniformity and similarity between the particles forms of synthesized haloperidol charge transfer complexes indicate that the existence of morphological phases of picric acid and TCNQ complexes have a homogeneous matrix. A spherical ball particles shape (Fig. 7a) is observed in case of the [(HPL)(PA)] with the particle size 5.0 μm. A homogeneous phase formation of [(HPL)(TCNQ)] complex has crack morphologies in the form of a dispersed with particle size 20 μm is exhibited in Fig. 7b. X-ray powder patterns of both representative haloperidol charge transfer complexes have given in Fig. 9a and b along with the prominent data. The peaks at $2\theta = 14^\circ$ and 16° are more target for the calculation of particle size, under Debye–Scherrer equation [41] using reflection from the XRD pattern. Debye–Scherrer equation is given by $D = 0.94\lambda/\beta\mathrm{Cos}\theta$, where D is size of the particles, λ is the wavelength of X-ray, β is the full width at half maximum (FWHM), and θ is the angle of the particles has been found to be 60 or 30 nm, respectively, for PA or TCNQ haloperidol charge transfer complexes.

3.6. Thermal and kinetic thermodynamic assessments

The data respected to the thermal decomposition of the synthetic haloperidol charge transfer complexes are discussed as it follows.

3.6.1. Thermal decomposition of [(HPL)(PA)] complex

The TG/DTG and DSC curves corresponding to the picric acid complex heated in the 30–1200 °C temperature range are exhibited in Fig. 10a. The thermal decomposition of [(HPL)(PA)] complex has only one very strong peak recorded in both DTG and DSC curves. This step is endothermic and assigned to the loss of organic moiety ($C_7H_{26}N_4O_9ClF$) with weight loss 60%.

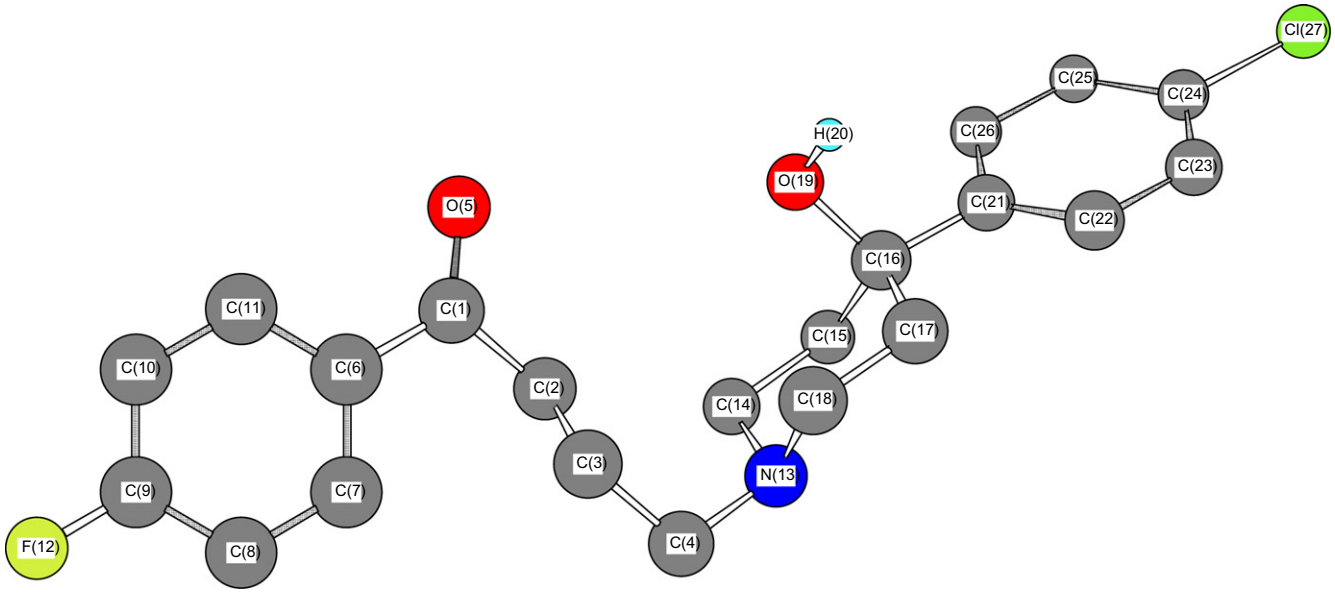

Fig. 12a. Optimized structure of haloperidol drug.

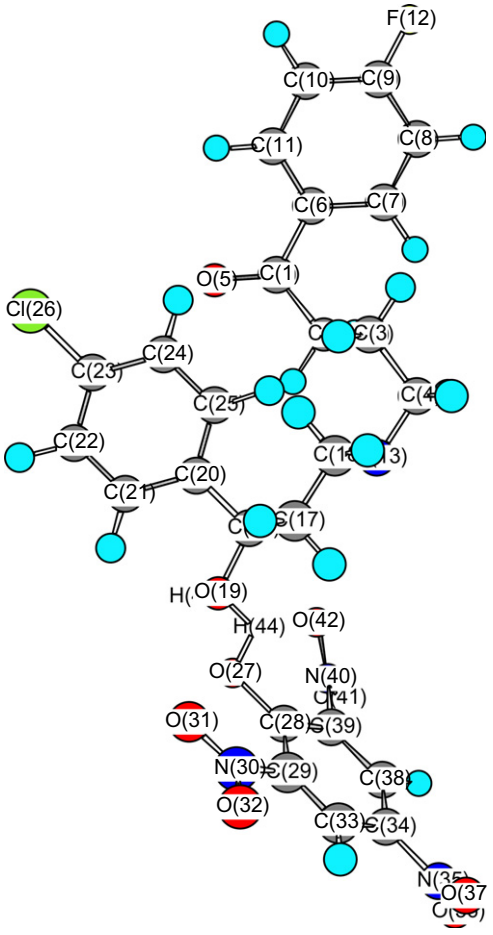

Fig. 12b. Optimized structure of [(HPL)(PA)] charge transfer complex.

3.6.2. Thermal decomposition of [(HPL)(TCNQ)] complex

Thermal analysis for [(HPL)(TCNQ)] complex has confirmed the thermal stability and the number of degradation steps upon to the DSC and DTG maximum peaks. According to TG and DSC curves (Fig. 10b) profiles this step comprises at least three decomposition steps at 150, 280, and 450 °C, first one is exothermic due to starting of melting points and decomposition, but the second and third endothermic process assigned to the completely decomposition of donor and acceptors with weight loss 68%.

In literature [42–44] there has been increasing interest in determining the rate-dependent parameters of solid-state non-isothermal decomposition reactions by analysis of TG curves. Several equations [42–44] have been proposed as means of analyzing a TG curve and obtaining values for kinetic parameters. Two major different methods (Horowitz and Metzger (HM) approximation method [43] and Coats and Redfern (CR) integral method [44]) are used for the evaluation of kinetic parameters. The enthalpy of activation, ΔH, and the free enthalpy of activation, ΔG, can be calculated via following equation

$$\Delta H = E - RT_m; \Delta G = \Delta H - T_m \Delta S \quad (8)$$

The kinetic parameters were evaluated using two of the above-mentioned methods by graphical means and are listed in Table 5. The satisfactory values of correlation coefficients (~1) in all cases indicates good agreement with experimented data and the values of kinetic parameters are reasonable and in good agreement. The calculated of activation energy ΔE^* values using Coats–Redfern and Horowitz–Metzger methods for the main decomposition stage of both haloperidol charge transfer complexes are found to be the average of E^*[(HPL)(PA)] = 132 kJ mol^{-1} > E^*[(HPL)(TCNQ)] = 98 kJ mol^{-1} which is in accordance with type of acceptors. The negative values of ΔS^* (Table 5) indicate that the reaction rates are slower than normal [45]. Furthermore, these data indicate that the activated complexes have more ordered structure than the reactants (see Fig 11).

3.7. Molecular modeling studies

Molecular modeling had been successfully used to detect three dimensional arrangements of atoms in free haloperidol drug and their charge transfer complexes. The bond lengths and bond angles values of the chelation complexes were summarized and refereed in Table 6 and Figs. 12a–c. This calculation for [(HPL)(PA)] and [(HPL)(TCNQ)] complexes were obtained by using the commercial available molecular modeling software Chem Office Ultra-7. These statistical data have a good agreement with formula 2 and 3 con-

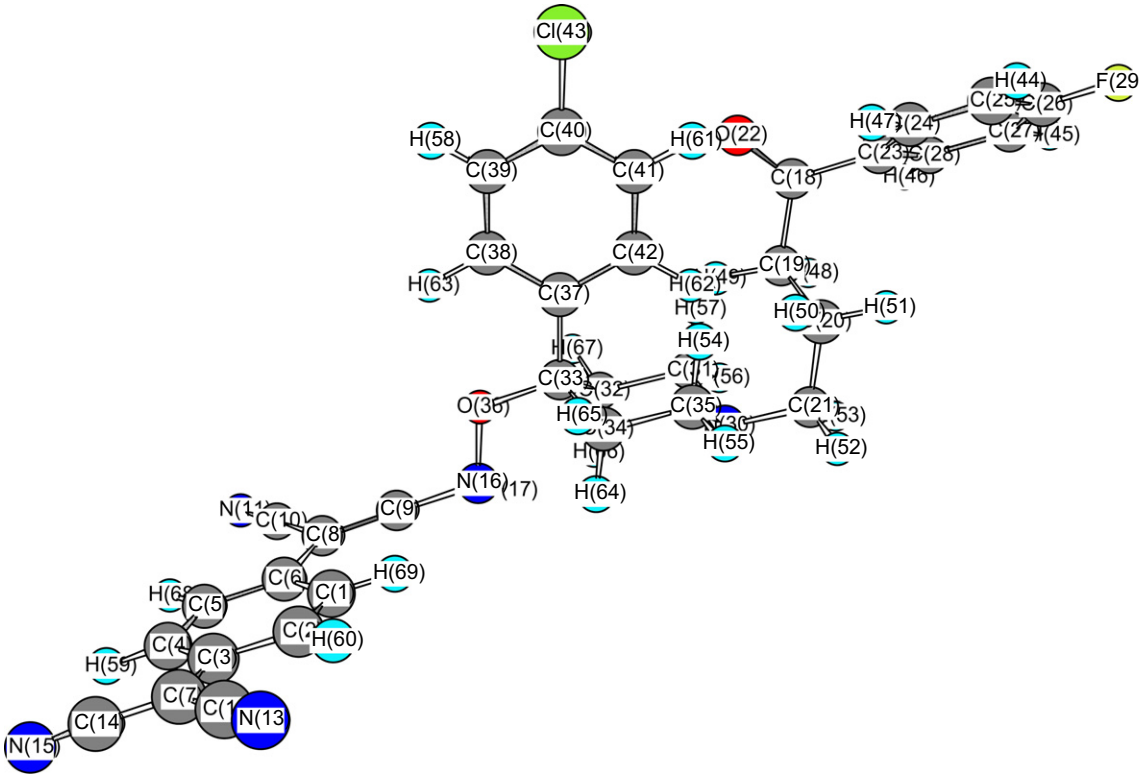

Fig. 12c. Optimized structure of [(HPL)(TCNQ)] charge transfer complex.

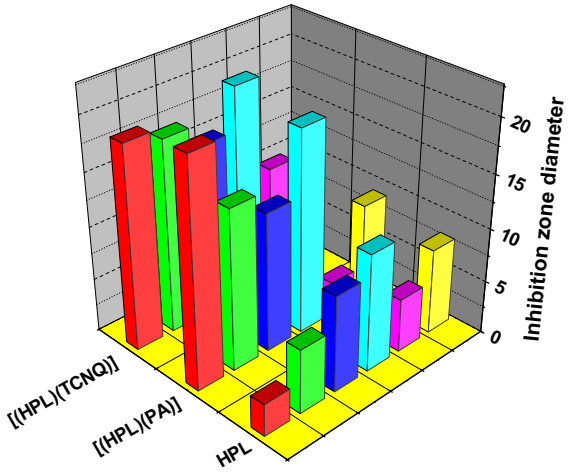

Fig. 13. Inhibition zone diameter of HPL, [(HPL)(PA)] and [(HPL)(TCNQ)] charge transfer complex.

firmed the presence of intermolecular hydrogen bonding between —OH of 4-hydroxy-1-piperidyl (drug donor) towards —OH of picric acid and one cyano group of TCNQ acceptors.

3.8. Biological activity studies

The biological assessment were studied in term antimicrobial activities of free haloperidol drug and their charge transfer complexes against gram-positive (*B. subtilis* and *S. aureus*) and gram-negative (*E. coli* and *P. aeruginosa*) and two strains of fungus (*A. flavus* and *C. albicans*). Result from the agar disc diffusion tests for antimicrobial activities of respective compounds are shown in Fig. 13. All tested compounds displayed a different degree of antimicrobial effect and both haloperidol charge transfer complexes displayed a degree of antimicrobial activities greater than free haloperidol drug donor against all organisms tested. The most reasons for lethal action of tested PA and TCNQ as well as similar charge transfer complexes reported in literature survey may be due to their interactions with critical interacellular sites causing the death of cells [46–49]. The variety of antimicrobial activities of tested compounds may due to a different degree of tested compounds penetration through cell membrane structure of target organism. In conclusion, the interaction between the HPL and π-acceptors in nano-structural form resulting developing of the effectiveness of biological characters of free drug.

4. Conclusion

The interactions between the electron donor haloperidol drug and the acceptors picric acid (PA) and 7,7′,8,8′-tetracyanoquinodimethane (TCNQ) were studied spectrophotometrically in methanol. New charge-transfer complexes were isolated and characterized through elemental analysis, (infrared, H NMR, electronic, and XRD spectra) as well as thermal and kinetic thermodynamic studies. The stoichiometry of the products was found to be 1:1 in all cases. Accordingly, the formed CT-complexes have the formulas [(HPL)(PA)] and [(HPL)(TCNQ)].

Acknowledgement

This work was supported by grants from Princess Nora Bint Abdul Rahman University, Riyadh, Saudi Arabia under project Grants No. 25/32.

References

[1] http://en.wikipedia.org.
[2] C.B. Joy, C.E. Adams, S.M. Lawrie, Irving, B. Claire, Cochrane Database Syst. Rev. 1 (4) (2006) CD003082, http://dx.doi.org/10.1002/14651858.CD003082.pub2.

[3] D.K. Roy, A. Saha, A.K. Mukherjee, Spectochim. Acta A 61 (2005) 2017.
[4] M.M.A. Hamed, M.I. Abdel-Hamid, M.R. Mahmoud, Monatsh. Chem. 129 (1998) 121.
[5] A. Dozal, H. Keyzer, H.K. Kim, W.W. Way, Int. J. Antimicrob. Agent 14 (2000) 261.
[6] R.S. Mulliken, J. Am. Chem. Soc. 72 (1950) 600.
[7] R.S. Mulliken, J. Am. Chem. Soc. 74 (1952) 811.
[8] M.S. Refat, L.A. El-Zayat, O.Z. Yeşilel, Spectrochim. Acta A 75 (2010) 745.
[9] M. Pandeeswaran, K.P. Elango, Spectrochim. Acta A 72 (2009) 789.
[10] A.S. Al-Attas, M.M. Habeeb, D.S. Al-Raimi, J. Mol. Liq. 148 (2009) 58.
[11] S.R. Lee, M.M. Rahman, K. Sawada, M. Ishida, Biosens. Bioelectron. 24 (2009) 1877.
[12] A.A. Attama, P.O. Nnamani, M.U. Adikwu, F.O. Akidi, Chem. Pharm. Bull. 52 (3) (2004) 303.
[13] H.F. Askal, Talanta 44 (10) (1997) 1749.
[14] K. Sharma, S.P. Sharma, S.C. Lahiri, Spectrochim. Acta A 92 (15) (2012) 212.
[15] K. Ganesh, C. Balraj, A. Satheshkumar, K.P. Elango, Spectrochim. Acta A 92 (15) (2012) 46.
[16] K. Ganesh, K.P. Elango, Spectrochim. Acta A 93 (2012) 185.
[17] A.W. Bauer, W.M. Kirby, C. Sherris, M. Turck, Am. J. Clin. Pathol. 45 (1966) 493.
[18] M.A. Pfaller, L. Burmeister, M.A. Bartlett, M.G. Rinaldi, J. Clin. Microbiol. 26 (1988) 1437.
[19] National Committee for Clinical Laboratory Standards, Performance Vol. Antimicrobial Susceptibility of Flavobacteria, 1997.
[20] National Committee for Clinical Laboratory Standards, Methods for Dilution Antimicrobial Susceptibility Tests for Bacteria that Grow Aerobically, Approved Standard M7–A3, National Committee for Clinical Laboratory Standards, Villanova, PA, 1993.
[21] National Committee for Clinical Laboratory Standards, Reference Method for Broth Dilution Antifungal Susceptibility Testing of Conidium-Forming Filamentous Fungi: Proposed Standard M38-A, NCCLS, Wayne, PA, USA, 2002.
[22] National Committee for Clinical Laboratory Standards, Methods for Antifungal Disk Diffusion Susceptibility Testing of Yeast: Proposed Guideline M44-P, NCCLS, Wayne, PA, USA, 2003.
[23] L.D. Liebowitz, H.R. Ashbee, E.G.V. Evans, Y. Chong, N. Mallatova, M. Zaidi, D. Gibbs, Global Antifungal Surveillance Group, Diagn. Microbiol. Infect. Dis. 4 (2001) 27.
[24] M.J. Matar, L. Ostrosky-Zeichner, V.L. Paetznick, J.R. Rodriguez, E. Chen, J.H. Rex, Antimicrob. Agents Chemother. 47 (2003) 1647.
[25] M.S. Refat, H.A. Saad, A.A. Adam, J. Mol. Str. 995 (1–3) (2011) 116.
[26] D.A. Skoog, Principle of Instrumental Analysis, third ed., Saunders College Publishing, New York, USA, 1985. Chapter 7.
[27] R. Abu-Eittah, F. Al-Sugeir, Can. J. Chem. 54 (1976) 3705.
[28] H. Tsubomura, R.P. Lang, J. Am. Chem. Soc. 86 (1964) 3930.
[29] W. Kiefer, H.J. Bernstein, Chem. Phys. Lett. 16 (1972) 5.
[30] L. Andrews, E.S. Prochaska, A. Loewenschuss, Inorg. Chem. 19 (1980) 463.
[31] K. Kaya, N. Mikami, Y. Udagawa, M. Ito, Chem. Phys. Lett. 16 (1972) 151.
[32] R. Rathone, S.V. Lindeman, J.K. Kochi, J. Am. Chem. Soc. 119 (1997) 9393.
[33] G. Briegleb, Z. Angew. Chem. 76 (1964) 326.
[34] G. Aloisi, S. Pignataro, J. Chem. Soc. Faraday Trans. 69 (1972) 534.
[35] G. Briegleb, J. Czekalla, Z. Physikchem. (Frankfurt) 24 (1960) 237.
[36] A.N. Martin, J. Swarbrick, A. Cammarata, Physical Pharmacy, third ed., Lee and Febiger, Philadelphia, PA, 1969. p. 344.
[37] L.J. Bellamy, The infrared Spectra of Complex Molecules, Chapman & Hall, London, 1975.
[38] R.D. Kross, V.A. Fassel, J. Am. Chem. Soc. 79 (1957) 38.
[39] S.E.J. Bell, N.M.S. Sirimuthu, Chem. Soc. Rev. 37 (2008) 1012.
[40] M.R. Kagan, R.L. McCreery, Anal. Chem. 66 (1994) 4159.
[41] A. Guinier, X-ray Diffraction, San Francisco, CA, 1963.
[42] E.S. Freeman, B. Carroll, J. Phys. Chem. 62 (1958) 91.
[43] H.H. Horowitz, G. Metzger, Anal. Chem. 35 (1963) 1464.
[44] A.W. Coats, J.P. Redfern, Nature 201 (1964) 68.
[45] A.A. Frost, R.G. Pearson, Kinetics and Mechanism, Wiley, New York, NY, USA, 1961.
[46] S.D. Cox, C.M. Mann, J.L. Markham, J.E. Gustafson, J.R. Warmington, S.G. Wyllie, Molecules 6 (2001) 87.
[47] I.M. Khan, A. Ahmad, M. Aatif, J. Photochem. Photobiol. B: Biol. 105 (2011) 6.
[48] I.M. Khan, A. Ahmad, M.F. Ullah, J. Photochem. Photobiol. B: Biol. 103 (2011) 42.
[49] I.M. Khan, A. Ahmad, J. Mol. Str. 977 (2010) 189.